

*ARMY RESEARCH LABORATORY*



## **Catalytic Combustion of Ethanol and Butanol**

**by Douglas A. Behrens and Ivan C. Lee**

---

**ARL-TN-0374**

**September 2009**

**Approved for public release; distribution unlimited.**

## **NOTICES**

### **Disclaimers**

The findings in this report are not to be construed as an official Department of the Army position unless so designated by other authorized documents.

Citation of manufacturer's or trade names does not constitute an official endorsement or approval of the use thereof.

Destroy this report when it is no longer needed. Do not return it to the originator.

# **Army Research Laboratory**

Adelphi, MD 20783-1197

---

---

**ARL-TN-0374**

**September 2009**

---

## **Catalytic Combustion of Ethanol and Butanol**

**Douglas A. Behrens and Ivan C. Lee**  
**Sensors and Electron Devices Directorate, ARL**

---

---

**Approved for public release; distribution unlimited.**

---

REPORT DOCUMENTATION PAGE			Form Approved OMB No. 0704-0188		
Public reporting burden for this collection of information is estimated to average 1 hour per response, including the time for reviewing instructions, searching existing data sources, gathering and maintaining the data needed, and completing and reviewing the collection information. Send comments regarding this burden estimate or any other aspect of this collection of information, including suggestions for reducing the burden, to Department of Defense, Washington Headquarters Services, Directorate for Information Operations and Reports (0704-0188), 1215 Jefferson Davis Highway, Suite 1204, Arlington, VA 22202-4302. Respondents should be aware that notwithstanding any other provision of law, no person shall be subject to any penalty for failing to comply with a collection of information if it does not display a currently valid OMB control number. <b>PLEASE DO NOT RETURN YOUR FORM TO THE ABOVE ADDRESS.</b>					
1. REPORT DATE (DD-MM-YYYY) September 2009		2. REPORT TYPE Final		3. DATES COVERED (From - To)	
4. TITLE AND SUBTITLE Catalytic Combustion of Ethanol and Butanol			5a. CONTRACT NUMBER		
			5b. GRANT NUMBER		
			5c. PROGRAM ELEMENT NUMBER		
6. AUTHOR(S) Douglas A. Behrens and Ivan C. Lee			5d. PROJECT NUMBER		
			5e. TASK NUMBER		
			5f. WORK UNIT NUMBER		
7. PERFORMING ORGANIZATION NAME(S) AND ADDRESS(ES) U.S. Army Research Laboratory ATTN: RDRL-SED-P 2800 Powder Mill Road Adelphi MD 20783-1197			8. PERFORMING ORGANIZATION REPORT NUMBER ARL-TN-0374		
9. SPONSORING/MONITORING AGENCY NAME(S) AND ADDRESS(ES)			10. SPONSOR/MONITOR'S ACRONYM(S)		
			11. SPONSOR/MONITOR'S REPORT NUMBER(S)		
12. DISTRIBUTION/AVAILABILITY STATEMENT Approved for public release; distribution unlimited.					
13. SUPPLEMENTARY NOTES					
14. ABSTRACT The combustion of energy dense liquid fuels in a catalytic micro-combustor is an attractive alternative to cumbersome batteries. To miniaturize the reactor, I developed an evaporation model to calculate the minimum distance required for complete droplet vaporization. By increasing the ambient temperature from 298 K to 325 K, the distance required for complete evaporation of a 6.5 micron droplet decreases from 3 to 0.15 cm. A platinum mesh acted as a baseline measurement and demonstrated 75% conversion of ethanol. I then selected a more active rhodium-coated alumina foam with a larger surface area and attained 100% conversion of ethanol and 95% conversion of butanol under fuel lean conditions. Effluent post-combustion gas analysis showed that varying the equivalence ratio results in two distinct regimes. A regime of high carbon selectivity for CO <sub>2</sub> occurs at low equivalence ratios and corresponds to complete combustion with a typical temperature of 775 K that is ideal for PbTe thermoelectric devices. Conversely, for equivalence ratios greater than 1, carbon selectivity for CO <sub>2</sub> decreases and hydrogen production increases. By tuning the equivalence ratio, I have shown that a single device can combust completely for thermoelectric applications, or operate as a fuel reformer to produce hydrogen gas for fuel cells.					
15. SUBJECT TERMS Alcohol, butanol, ethanol, microburner, combustion					
16. SECURITY CLASSIFICATION OF:			17. LIMITATION OF ABSTRACT UU	18. NUMBER OF PAGES 22	19a. NAME OF RESPONSIBLE PERSON Ivan C. Lee
a. REPORT Unclassified	b. ABSTRACT Unclassified	c. THIS PAGE Unclassified			19b. TELEPHONE NUMBER (Include area code) (301) 394-0292

---

## Contents

---

<b>List of Figures</b>	<b>iv</b>
<b>1. Introduction</b>	<b>1</b>
<b>2. Experimental Approach</b>	<b>3</b>
2.1 Modeling Approach.....	4
2.2 Modeling Results.....	5
2.3 Experimental Results.....	7
<b>3. Discussion</b>	<b>11</b>
<b>4. Conclusions</b>	<b>12</b>
<b>5. References</b>	<b>13</b>
<b>List of Symbols, Acronyms, and Abbreviations</b>	<b>14</b>
<b>Distribution</b>	<b>15</b>

---

## List of Figures

---

Figure 1. Chemical structures of ethanol and n-butanol. Gray, black, and red molecules represent hydrogen carbon, and oxygen atoms respectively. Courtesy of Wikipedia.org.....	1
Figure 2. Taylor cone depiction at steady state. Picture courtesy of Wikimedia.org.....	2
Figure 3. Reactor schematic.....	4
Figure 4. Droplet with coordinate system ( <i>II</i> )......	5
Figure 5. $D^2$ law model for ethanol droplet. ....	6
Figure 6. Droplet lifetime as a function of initial droplet diameter for ethanol.....	7
Figure 7. Ethanol and butanol conversion with Pt mesh and Rh/Al <sub>2</sub> O <sub>3</sub> foam catalysts. ....	8
Figure 8. Carbon selectivity for ethanol with a Rh/Al <sub>2</sub> O <sub>3</sub> foam catalyst as a function of equivalence ratio. ....	8
Figure 9. Carbon selectivity for butanol with a Rh/Al <sub>2</sub> O <sub>3</sub> foam catalyst as a function of equivalence ratio. ....	9
Figure 10. Hydrogen selectivity for ethanol with a Rh/Al <sub>2</sub> O <sub>3</sub> foam catalyst as a function of equivalence ratio. ....	9
Figure 11. Hydrogen selectivity for butanol with a Rh/Al <sub>2</sub> O <sub>3</sub> foam catalyst as a function of equivalence ratio. ....	10
Figure 12. Hydrogen selectivity for ethanol and butanol with a Rh/Al <sub>2</sub> O <sub>3</sub> foam catalyst as a function of equivalence ratio. ....	10

---

## 1. Introduction

---

With the ever-increasing amount of technology a Soldier is required to carry on the battlefield comes an inevitable increase in the size and weight of the corresponding power source. Battery technology has made great strides in the past decades, resulting in new anodes, cathodes, and the ability to recharge them. However, batteries have an extremely small energy density when compared to liquid fuels such as ethanol, butanol, and JP8. A typical lithium (Li) ion battery is roughly two orders of magnitude less dense than ethanol or butanol—0.6 MJ/kg compared to 29 and 36.6 MJ/kg. If an efficient method for combusting these fuels at temperatures in the range of thermoelectric or other energy converting devices was developed, the power source could be drastically miniaturized, which would significantly decrease the load a Soldier must carry.

Alcohols such as ethanol and butanol, see figure 1, were chosen because they have several characteristics that are ideal for experimentation.

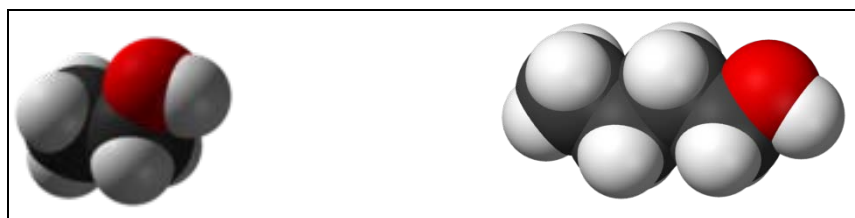


Figure 1. Chemical structures of ethanol and n-butanol. Gray, black, and red molecules represent hydrogen carbon, and oxygen atoms respectively. Courtesy of Wikipedia.org

They are easily renewable from biomass and possess a simple chemical structure. The increase in energy density can only be exploited if the fuel is in the energy-rich liquid phase at the conditions under which it is to be used. Ethanol and butanol are both liquids at room temperature and don't boil until 78.4 °C and 117.7 °C, respectively. The alcohols are single components, not a combination of components with different boiling points and viscosities. This enables simpler evaporation and diffusion models to predict their behavior. Since complete combustion results in the production of carbon dioxide (CO<sub>2</sub>) and water, the fuels burn clean. Neither of these combustion products poisons the catalyst, so operation with the same catalyst can continue for longer periods of time. Also, they are electrically conductive enough that they can form a Taylor Cone when subjected to a voltage differential. The Taylor cone formation allows for a steady-state evaporation rate to be established, and is shown in figure 2.

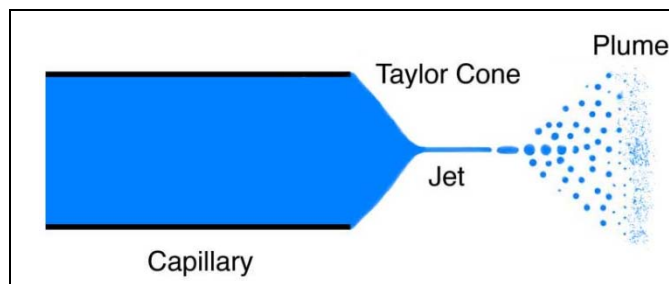
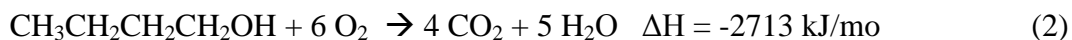


Figure 2. Taylor cone depiction at steady state. Picture courtesy of Wikimedia.org.

The combustion of ethanol and butanol occur via equations 1 and 2 and are extremely exothermic.



The equivalence ratio ( $\phi$ ), the ratio of the actual fuel-to-air ratio divided by the stoichiometric fuel-to-air ratio, also plays an important role. A  $\phi$ -value of unity signifies a stoichiometric feed of fuel and air, as shown in equations 1 and 2. The  $\phi$ -value can be controlled by adjusting the amount of ethanol or oxygen that is reacted. In the limit of high  $\phi$ -values, the reaction is “fuel rich” and thermal decomposition or fuel reformation occurs because not enough oxygen exists to combust the fuel. However, low  $\phi$ -values indicate a “fuel lean” reaction that contains plenty of oxygen to oxidize the fuel into its combustion products—carbon dioxide and water.

The chemical kinetics of high temperature ethanol oxidation reactions have been exhaustively studied for temperatures ranging from 800–1600 K, for equivalence ratios varying from 0.25–2 (1–3). The experimental findings match the predicted theory with remarkable agreement, even over this extremely wide range of temperatures. Ethanol decomposition reaction pathways through use of pyrolysis—with no oxygen present—have also been studied in depth for temperatures greater than 900 K (4, 5).

Homogeneous gas phase flame-combustion reactions were carried out in the literature (6, 7), but temperatures for these types of reactions can exceed 2000 K, which is far too high for any economically viable energy conversion device. Catalytic combustion of a more complicated and energy dense hydrocarbon, JP8, achieved complete combustion for flowrates less than 5 mL/h at a maximum catalyst temperature of less than 900 K (8). This indicated that the catalytic reactions do not only initiate the reaction, but play a large role in overall fuel conversion. Experiments have also shown that miniaturizing the reactor can require use of a catalyst. This results from the larger surface effects as an increasing surface area/volume ratio is realized as the overall size is decreased (9). Without the catalyst to support the combustion at lower

temperatures, the possibility exists that the larger convection forces would extinguish the reaction.

The optimization of catalysts for different fuels is also an active area of research. Experiments have been conducted with catalysts composed of thermally stabilized, ion-exchanged zeolite, palladium on stabilized alumina, and catalysts doped with cerium (Ce) and nickel (Ni) to better prevent sulfur poisoning when using JP8 (8, 10). As shown above, catalysts can lower the activation barrier of a reaction, thus allowing the reaction pathway to occur at lower temperatures. This is extremely advantageous because it allows for combustion temperatures between 675 K and 875 K, which is ideal for lead telluride (PbTe) thermoelectric devices.

There are, however, significant challenges that lie ahead before liquid fuels can be commercially viable. The Li ion battery is widely used, not because of its size or weight, but because of its durability, ease of integration into many electronic technologies, and affordability. Liquid fuels need to become more reliably combustible, more rigid in structure, and have a consistent and efficient method to convert the products produced into an applicable form of energy.

---

## 2. Experimental Approach

---

A grounded mesh was placed at a distance of 1 cm below the droplet source (a stainless steel tube) in a cylindrical quartz reactor, and the catalyst was located about 12.5 cm below the bottom of the grounded mesh. Care was taken to make certain that the grounded mesh was perpendicular to the direction of the droplet velocity so as to create a uniform electric field. Nitrogen and oxygen gases were introduced near the top of the reactor, and the effluent gas was sent to the gas chromatograph (GC) through the bottom. Liquid fuel entered the reactor via a stainless steel tube and was formed into a Taylor Cone by creating a voltage difference between the droplet source and a neutral grounded mesh ( $\approx 3300$  V). Sufficient heat was supplied via heating tape to the grounded mesh (generally a couple degrees above the boiling point of the fuel to account for any impurities) to ensure complete evaporation, and to the catalyst to ensure that temperatures were high enough to support catalytic activity. The catalyst material was placed between two inert, porous alumina supports that acted as a heat shield and also ensured uniform fuel vapor concentration over the entire catalyst surface. The platinum mesh weighed about 0.50 g and was roughly 0.5 mm thick. The rhodium (Rh)/aluminum oxide ( $\text{Al}_2\text{O}_3$ ) foam contained 0.061 g of Rh and was prepared in the manner detailed in the literature (10). Details are depicted in figure 3.

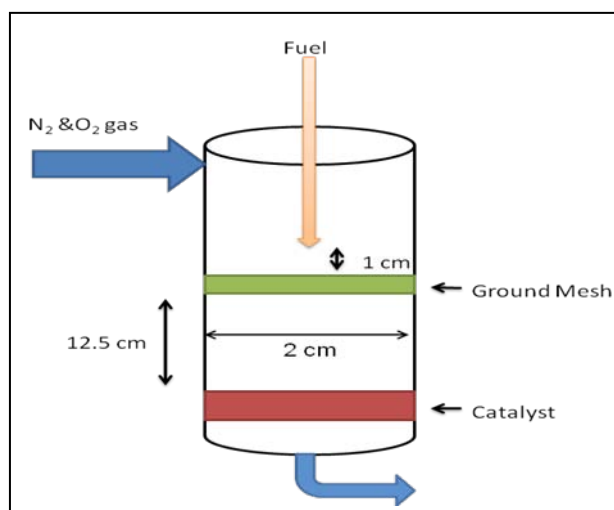


Figure 3. Reactor schematic.

Since analysis of the combustion products is crucial to understanding the results of the operating conditions, an air-tight seal was needed around the combustor and GC. Before each experiment, nitrogen gas was passed through the reactor in order to clear out any lingering gases, and to ensure that there was no leak and that no oxygen was present. The heat source was activated, the appropriate nitrogen and oxygen flowrates were introduced, and the ground and catalyst temperatures were allowed to equilibrate. Then the voltage differential between the ground and the stainless steel tube was established, and the fuel flow was initiated. Voltages were then adjusted to maintain Taylor cone stability as needed. The ground and catalyst temperatures were again allowed to reach a steady-state operating temperature, and the GC recorded the gas composition during this time. Ethanol was the main experimental fuel because it formed more stable Taylor cones because of its high electrical conductivity, and butanol was tested for comparison purposes. When we compared ethanol and butanol, the experiments were run at the same equivalence ratios. This set the total oxygen flowrate, and then the nitrogen flowrate was adjusted so that the total volumetric flowrate of gas remained the same. This guaranteed that the residence time inside the reactor was the same for both fuels, thus eliminating other variables that could cloud the results. Fuel flowrates on the order of 1 mL/h were used.

## 2.1 Modeling Approach

In order to predict the evolution of the droplet size with time, the Stefan Problem's differential mass balance was solved for binary species in a spherically symmetric coordinate system, with the radius being the only coordinate variable, as shown in figure 4 (11).

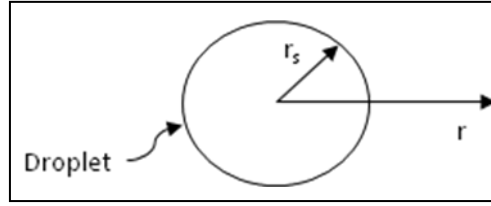


Figure 4. Droplet with coordinate system (11).

Using the droplet mass conservation, the change in droplet mass with time is equal to the rate at which the liquid is vaporized, as shown in equation 3.

$$\frac{dm_d}{dt} = -\dot{m} \quad (3)$$

Here,  $\dot{m}$  represents the evaporation rate and is attained, in part, by assuming that at the droplet surface, the vapor mass fraction is  $Y_{A,s}$ . This is shown in equation 4.

$$\dot{m} = 4\pi r_s \rho D_{AB} \ln\left(\frac{1-Y_{A,\infty}}{1-Y_{A,s}}\right) \quad (4)$$

Where  $r_s$ , represents the droplet radius at the surface,  $\rho$  represents the gas density,  $D_{AB}$  represents the binary diffusion coefficient, and the vapor fraction at the droplet surface and an infinite distance away are  $Y_{A,s}$  and  $Y_{A,\infty}$ , respectively. The mass of the droplet is simply the volume multiplied by the density. Plugging both this relationship and equation 4 into equation 3, and rearranging, yields equation 5.

$$\frac{dD^2}{dt} = -\frac{8\rho D_{AB}}{\rho_l} \ln(1 + B_y) \quad (5)$$

Here the natural log term was rewritten from the form seen in equation 4. Then, by defining the right-hand side of equation 5 as a constant  $K$ , the equation can be integrated with the appropriate boundary conditions, as in equation 6.

$$D^2(t) = D_0^2 - Kt \quad (6)$$

Equation 6, also known as the  $D^2$  law, shows that setting a  $D$  value of zero and solving for  $t$  would represent the time it takes for the droplet to completely evaporate. The  $D^2$  law has been experimentally verified for initial ethanol droplet diameters ranging from 0.93 mm to 5.83 mm (12). The correlation also holds for droplets in the micron diameter range, though they weren't explicitly studied in that report. Implicit in the derivation of the above model is that the ambient temperature not exceed the boiling point of the droplet. This assumption eliminated the need to apply an energy balance to the liquid droplet or the gas envelope surrounding the droplet, greatly simplifying the number of equations and unknowns in the process.

## 2.2 Modeling Results

Phase Doppler Imaging showed that the initial droplet size coming out of the stainless steel tube used for the experiment was roughly 6.5 microns in diameter and had a velocity of

approximately 10 m/s. Accordingly, equation 6 was solved for a 6.5 micron ethanol droplet at various temperatures and was plotted in figure 5.

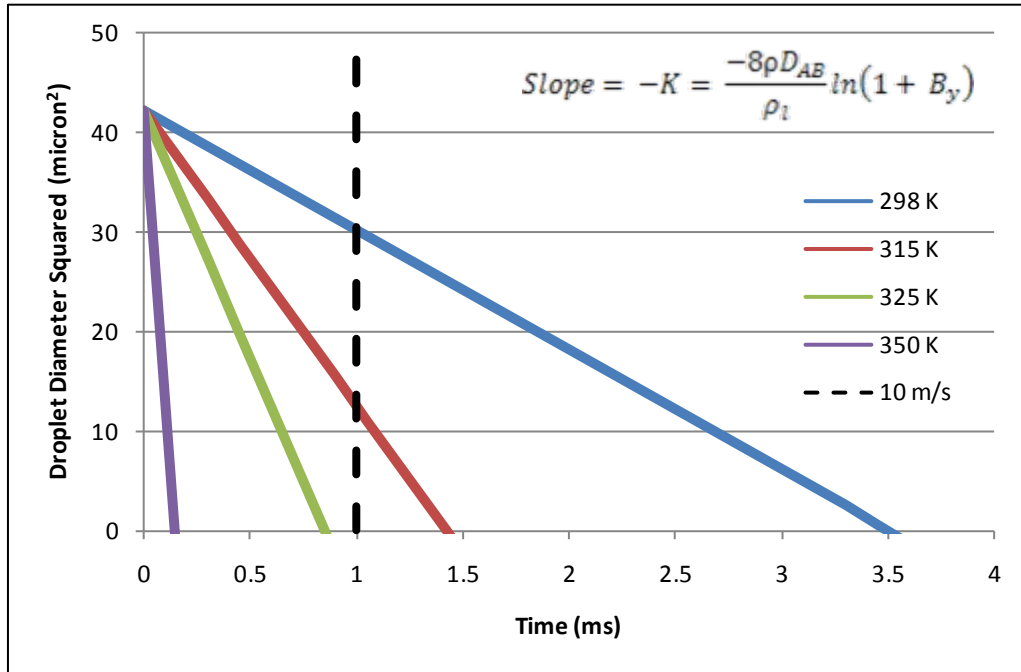


Figure 5.  $D^2$  law model for ethanol droplet.

Figure 5 shows the droplet evolution as a function of time for an ethanol droplet with an initial diameter of 6.5 microns (42.25 square microns) for temperatures ranging from room temperature up to the boiling point of ethanol. Each line follows a single droplet from its initial release until complete evaporation (intersection with the x-axis). The black dash indicates the time it would take for a droplet traveling at 10 m/s (anticipated velocity) to cover the 1 cm gap and reach the grounded mesh. The graph shows that at room temperature the droplet does not fully vaporize before hitting the grounded screen, whereas a temperature of 350 K would clearly result in complete evaporation before the grounded mesh is reached. Since the operating temperature for the reactor is right around the boiling point of the fuel—about 350 K—the model ensures that the droplet will be completely vaporized. Also, it can be seen that an increase in temperature from 298 K to 325 K reduces the droplet lifetime from 3.5 s to less than 1 s. An increase in temperature to 350 K would create complete evaporation in less than 1 s.

The model can also predict the droplet lifetime as a function of initial droplet diameter, as shown in figure 6.

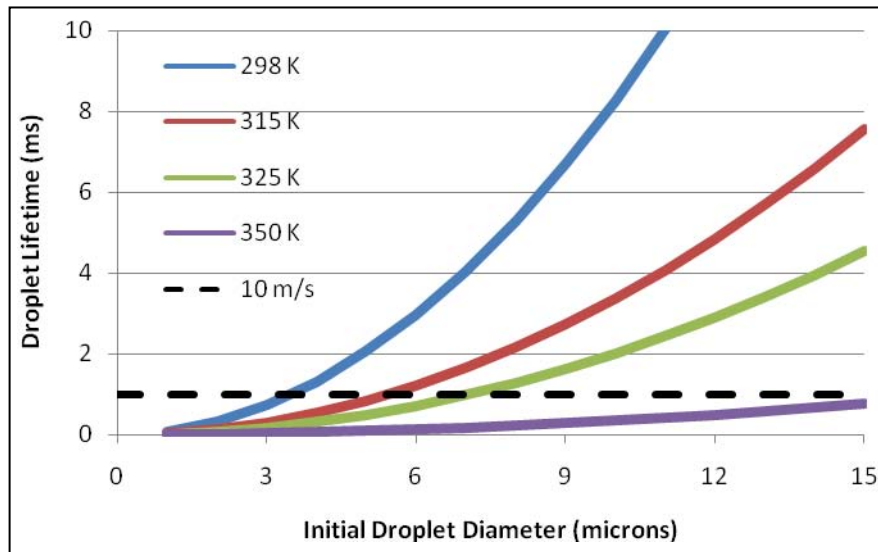


Figure 6. Droplet lifetime as a function of initial droplet diameter for ethanol.

The dashed line again represents how long it would take for a droplet moving at 10 m/s to reach the grounded mesh positioned 1 cm away. The graph shows that for a diameter of 2 microns, the droplet would be evaporated over the entire range of temperatures shown. Conversely, for an initial droplet size of 12 microns, only a temperature of 350 K would result in complete evaporation before the grounded screen. This was used to determine how much heat needed to be supplied in order to achieve complete evaporation for the given initial droplet diameter. Together, these graphs obtained from the model drove the design considerations by limiting how small the reactor could be based on droplet diameters and operation temperatures, as well as how much heat was required to achieve these goals.

### 2.3 Experimental Results

Figure 7 shows the conversion for ethanol and butanol combustion as a function of equivalence ratio. Ethanol combustion data were obtained for both the Pt mesh and Rh/Al<sub>2</sub>O<sub>3</sub> foam catalysts, whereas the Rh/Al<sub>2</sub>O<sub>3</sub> foam was the only catalyst used for butanol combustion.

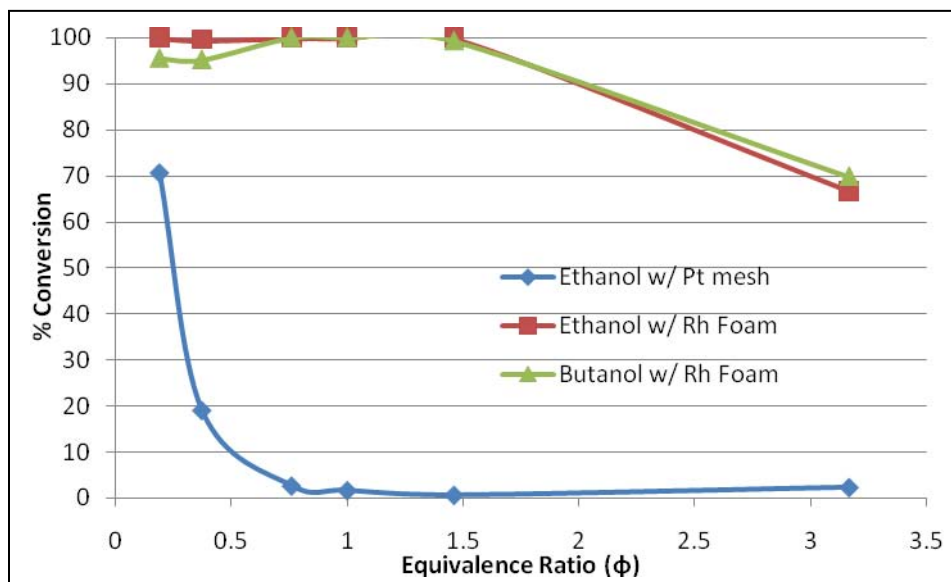


Figure 7. Ethanol and butanol conversion with Pt mesh and Rh/ $\text{Al}_2\text{O}_3$  foam catalysts.

Figure 8 displays the carbon selectivity of ethanol combustion for carbon monoxide, carbon dioxide, paraffins, and olefins, with increasing equivalence ratios. Here, paraffins are defined as any hydrocarbon chains made up of only single carbon-to-carbon bonds, whereas olefins are any hydrocarbon chains that have a double bond linking carbons together.

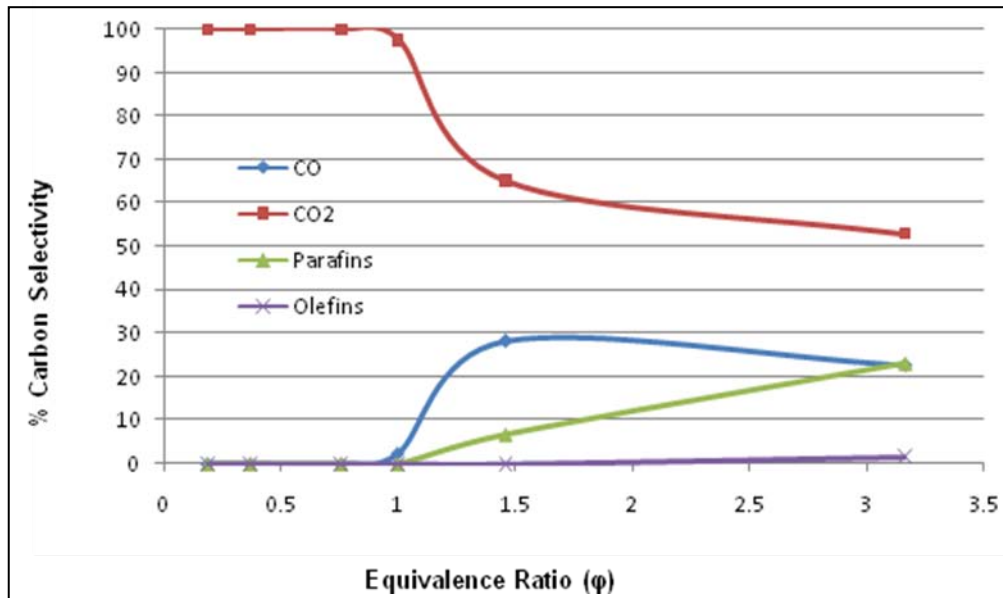


Figure 8. Carbon selectivity for ethanol with a Rh/ $\text{Al}_2\text{O}_3$  foam catalyst as a function of equivalence ratio.

The carbon selectivity data for butanol combustion is depicted in figure 9 in an analogous manner to figure 8. Again, the definition of paraffins and olefins remains the same as it was defined earlier.

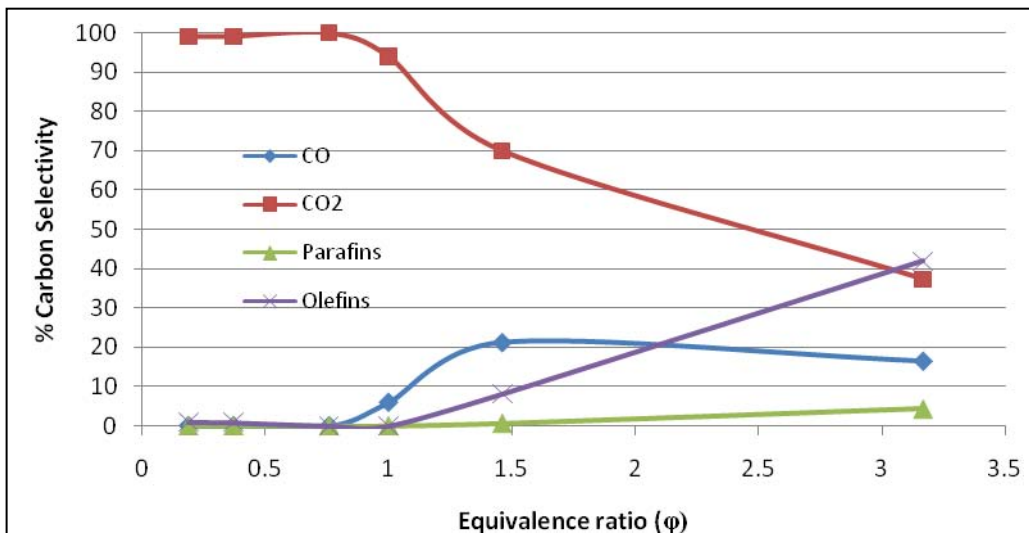


Figure 9. Carbon selectivity for butanol with a Rh/Al<sub>2</sub>O<sub>3</sub> foam catalyst as a function of equivalence ratio.

Hydrogen selectivity data for ethanol combustion is depicted in figure 10 as a function of equivalence ratio. Data for hydrogen gas, water vapor, paraffins, and olefins are reported.

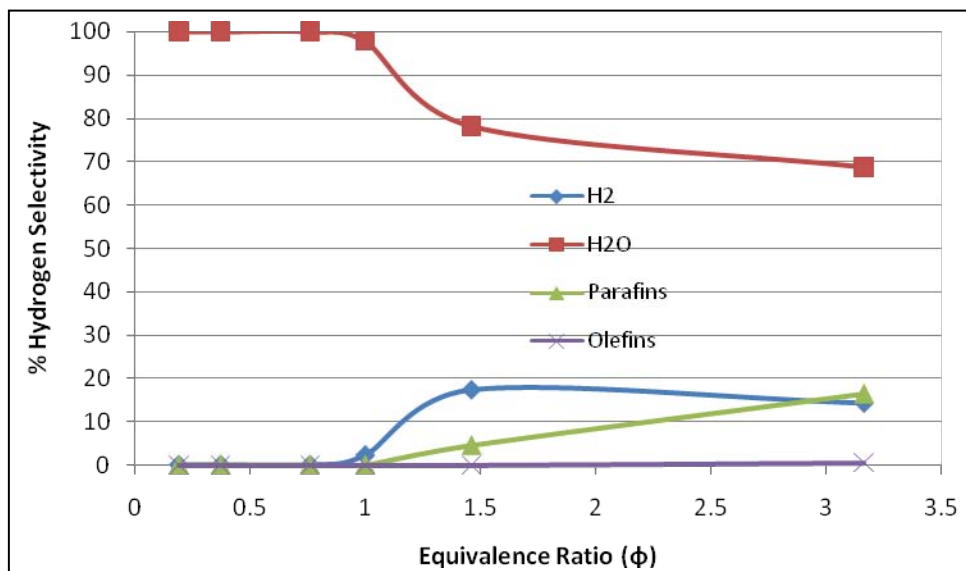


Figure 10. Hydrogen selectivity for ethanol with a Rh/Al<sub>2</sub>O<sub>3</sub> foam catalyst as a function of equivalence ratio.

Figure 11 details the hydrogen selectivity data for butanol combustion in a similar manner to that in figure 10.

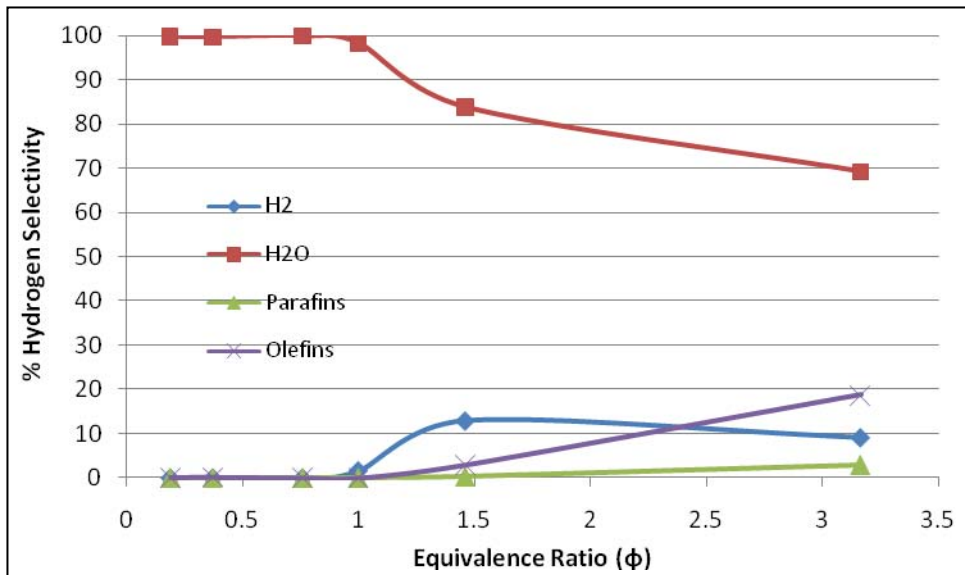


Figure 11. Hydrogen selectivity for butanol with a Rh/Al<sub>2</sub>O<sub>3</sub> foam catalyst as a function of equivalence ratio.

Figure 12 compares the hydrogen selectivity for ethanol and butanol as a function of equivalence ratio. The experiments for ethanol and butanol were both done using the Rh/Al<sub>2</sub>O<sub>3</sub> foam catalyst.

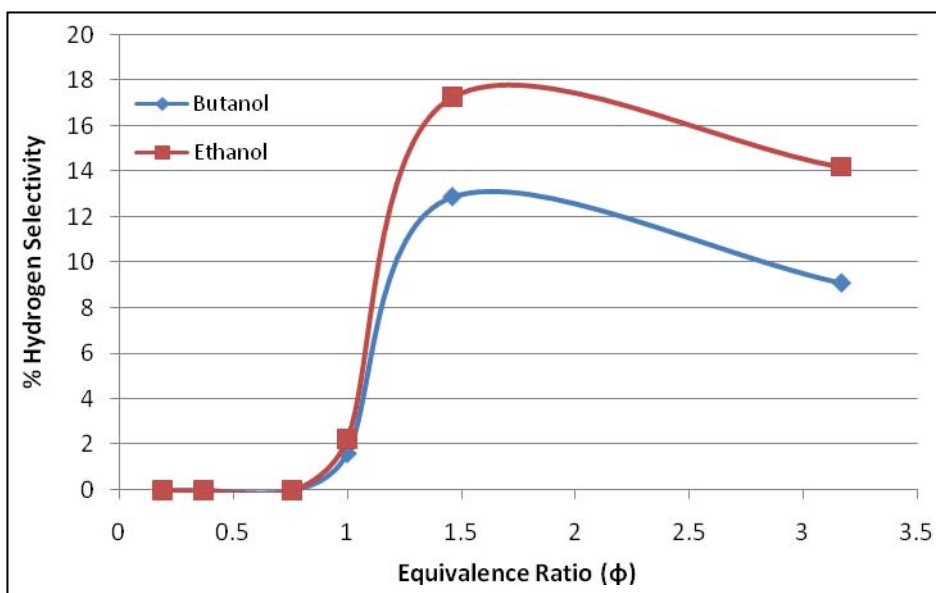


Figure 12. Hydrogen selectivity for ethanol and butanol with a Rh/Al<sub>2</sub>O<sub>3</sub> foam catalyst as a function of equivalence ratio.

---

### 3. Discussion

---

Figure 7 shows that the Rh/Al<sub>2</sub>O<sub>3</sub> foam catalyst is superior to the platinum mesh. The foam was able to achieve almost 100% conversion for low equivalence ratios while maintaining greater than 60% conversion at high equivalence ratios (excess fuel). On the other hand, the platinum mesh was able to achieve 70% conversion at very low equivalence ratios, but the conversion quickly decreased to less than 5% as the fuel-to-air ratio was increased. This trend is likely due to the higher catalytic activity of the Rh/Al<sub>2</sub>O<sub>3</sub> foam, as well as the fact that the foam had a larger surface area for reactions to take place. In addition, Rh particles were evenly dispersed over the Al<sub>2</sub>O<sub>3</sub> surface so that the entire surface area could be effectively used.

Examination of figure 8 shows that two distinct regimes exist for carbon selectivity. At low equivalence ratios, where excess oxygen is present, the selectivity of carbon to CO<sub>2</sub> is 100%. This is partly due to the fact that any carbon monoxide (CO) produced will be immediately oxidized by the excess oxygen into CO<sub>2</sub>. If CO<sub>2</sub> is produced, it means that combustion is occurring and that water is the other product. Since those are the only products produced at low equivalence ratios, this is the regime of complete combustion. As the equivalence ratio approaches unity—i.e., there are 3 moles of oxygen for every mole of ethanol (equation 1)—the selectivity of carbon for CO<sub>2</sub> starts to decrease. As the ratio of ethanol to oxygen is increased further, more carbon monoxide, methane, and even ethene are produced as the carbon selectivity of carbon dioxide decreases. The appearance of significant amounts of CO indicates that the fuel is now being reformed into CO and H<sub>2</sub>. This has strong possibilities for applications in fuel cells, and the poisonous CO can be easily neutralized through the water gas-shift reaction that converts CO and H<sub>2</sub>O into CO<sub>2</sub> and more H<sub>2</sub>.

Figure 9 shows the carbon selectivities for butanol combustion, and the trend is very similar to that of ethanol, shown in figure 8. CO<sub>2</sub> has a nearly 100% carbon selectivity until the stoichiometric fuel-to-air ratio is approached. After that, the CO<sub>2</sub> selectivity rapidly decreases to a final value of less than 40%. Comparison of figures 8 and 9 show that the carbon selectivity for CO<sub>2</sub> decreases much further for butanol than for ethanol combustion, and this corresponds to larger amounts of other products being produced. About 60% of the carbons for butanol combustion compared to only about 45% of the carbons in ethanol combustion are found in a compound other than CO<sub>2</sub> at an equivalence ratio of 3.17. The comparison also indicates that olefins (double-bonded carbon chains) are produced for butanol combustion in significant amounts, whereas only trace amounts of olefins were produced for ethanol combustion. The converse is true of paraffins (single bonded carbon chains); more paraffins are found for ethanol than are found for butanol combustion. Further research needs to be conducted in order to fully understand the mechanism that produces these results.

Figure 10 depicts the hydrogen selectivity for ethanol combustion, and shows that nearly all of the hydrogen atoms are present as water vapor at low equivalence ratios. Then, as the stoichiometric ratio is approached and the equivalence ratio increases further, more hydrogen gas and paraffins were produced, as less and less water vapor is produced. However, even at equivalence ratios greater than 3, the hydrogen selectivity for water vapor is still around 70%. Hydrogen selectivity for H<sub>2</sub> was about 18% and occurred for an equivalence ratio of roughly 1.5. Hydrogen selectivity for paraffins was the highest at the largest equivalence ratio studied, and only trace amounts of olefins were detected.

The hydrogen selectivities for butanol are shown in figure 11. The graph looks strikingly similar to the hydrogen selectivity for ethanol. The hydrogen selectivity for water vapor begins to decrease around the stoichiometric ratio, but decreases to a final value of around 70%. Hydrogen gas selectivity increases for  $\phi$ -values greater than one, and then decreases slightly to a final value of between 15% and 10%, respectively, for ethanol and butanol combustion. The main difference is the amount of olefins and paraffins produced. Ethanol combustion produced a hydrogen selectivity of nearly 20% paraffins and no olefins at a  $\phi$ -value of 3.17, whereas butanol combustion produced a hydrogen selectivity of slightly less than 20% olefins and about 3% paraffins. Further research into the reaction mechanism is required before this trend can be completely understood.

Figure 12 displays a comparison between the hydrogen selectivities for ethanol and butanol combustion on the same graph. This graph indicates that ethanol combustion produces a higher hydrogen selectivity for H<sub>2</sub> gas at all equivalence ratios. More importantly, an optimum equivalence ratio of approximately 1.5 produces the highest hydrogen selectivity for both ethanol and butanol. Thus, this would be an ideal equivalence ratio at which to operate if H<sub>2</sub> production for fuel cells was required.

---

## 4. Conclusions

---

An evaporation model was used to predict the behavior of ethanol droplets at varying temperatures. This model limited how small the reactor could be made based on the velocity of the fuel droplets and the temperature of operation. From this, the temperature required to evaporate a droplet of a given initial diameter was calculated to make sure that it fully vaporized before reaching the grounded mesh. A comparison between a platinum mesh and Rh/Al<sub>2</sub>O<sub>3</sub> foam indicated that the foam was more catalytically active over all equivalence ratios and, thus, yielded higher conversions. The microcombustor was then shown to be able to produce complete combustion products and the associated high temperatures for pairing with thermoelectric devices at low equivalence ratios. The same device can also be used to achieve fuel reformation for hydrogen fuel cells at higher equivalence ratios by changing only the fuel-to-air ratio.

---

## 5. References

---

1. Dunphy, M. P.; Patterson, P. M.; Simmie, J. M. High-temperature Oxidation of Ethanol. *J. CHEM. SOC.* **1991**, 2549–4559.
2. Li, J.; Kazakov, A.; Chaos, M.; Dryer, F. L. Chemical Kinetics of Ethanol Oxidation. *5th US Combustion Meeting*. San Diego 2007.
3. Norton, T. S.; Dryer, F. L. An Experimental and Modeling Study of Ethanol Oxidation Kinetics in an Atmospheric Pressure Flow Reactor. *International Journal of Chemical Kinetics* **1992**, 319–344.
4. Li, J.; Kazakov, A.; Dryer, F. L. Experimental and Numerical Studies of Ethanol Decomposition Reactions. *J. Phys. Chem* **2004**, 7671–7680.
5. Borisov, A. A.; Zamanskii, V. M.; Konnov, A. A.; Lisyanskii, V. V.; Rusakov, S. A.; Skachkov, G. I. A Mechanism of High-temperature Ethanol Ignition. *Sov. J. Chem. Phys.* **1992**, 2527–2537.
6. Anderson, E. K.; Koch, J. A.; Kyritsis, D. C. Phenomenology of Electrostatically Charged Droplet Combustion in Normal Gravity. *Combustion and Flame* **2008**, 624–629.
7. Parag, S.; Raghavan, V. Experimental Investigation of Burning Rates of Pure Ethanol and Ethanol Blended Fuels. *Combustion and Flame* **2008**, 997–1005.
8. Kyritsis, D. C.; Coriton, B.; Faure, F.; Roychoudhury, S.; Gomez, A. Optimization of a Catalytic Combustor Using Electrosprayed Liquid Hydrocarbons for Mesoscale Power Generation. *Combustion and Flame* **2004**, 77–89.
9. Gomez, A.; Berry, J. J.; Roychoudhury, S.; Coriton, B.; Huth, J. From Jet Fuel to Electric Power Using a Mesoscale, Efficient Stirling Cycle. *Proceedings of the Combustion Institute* **2007**, 3521–3259.
10. Lee, I. C. Rhodium Supported on Thermally Enhanced Zeolite as Catalysts for Fuel Reforming of Jet Fuel. *Catalysis Today* **2008**, 258–265.
11. Turns, S. R. *An Introduction of Combustion 2nd Edition*. Boston: McGraw-Hill 2006.
12. Kazakov, A., Conley, J., & Dryer, F. L. Detailed Modeling of an Isolated, Ethanol Droplet Combustion Under Microgravity Conditions. *Combustion and Flame* **2003**, 301–314.

---

## List of Symbols, Acronyms, and Abbreviations

---

Al <sub>2</sub> O <sub>3</sub>	Aluminum oxide
CO	Carbon monoxide
CO <sub>2</sub>	Carbon dioxide
Ce	Cerium
GC	Gas chromatograph
Li	lithium
PbTe	Lead telluride
Ni	Nickel
Rh	Rhodium

<u>No of</u> <u>Copies</u>	<u>Organization</u>
1 ELECT	ADMNSTR DEFNS TECHL INFO CTR ATTN DTIC OCP 8725 JOHN J KINGMAN RD STE 0944 FT BELVOIR VA 22060-6218
1	DARPA ATTN IXO S WELBY 3701 N FAIRFAX DR ARLINGTON VA 22203-1714
1 CD	OFC OF THE SECY OF DEFNS ATTN ODDRE (R&AT) THE PENTAGON WASHINGTON DC 20301-3080
1	US ARMY RSRCH DEV AND ENGRG CMND ARMAMENT RSRCH DEV AND ENGRG CTR ARMAMENT ENGRG AND TECHNLY CTR ATTN AMSRD AAR AEF T J MATTS BLDG 305 ABERDEEN PROVING GROUND MD 21005-5001
1	PM TMS, PROFILER (MMS-P) AN/TMQ-52 ATTN B GRIFFIES BUILDING 563 FT MONMOUTH NJ 07703

<u>No of</u> <u>Copies</u>	<u>Organization</u>
1	US ARMY INFO SYS ENGRG CMND ATTN AMSEL IE TD A RIVERA FT HUACHUCA AZ 85613-5300
1	COMMANDER US ARMY RDECOM ATTN AMSRD AMR W C MCCORKLE 5400 FOWLER RD REDSTONE ARSENAL AL 35898-5000
1	US GOVERNMENT PRINT OFF DEPOSITORY RECEIVING SECTION ATTN MAIL STOP IDAD J TATE 732 NORTH CAPITOL ST NW WASHINGTON DC 20402
1	US ARMY RSRCH LAB ATTN RDRL CIM G T LANDFRIED BLDG 4600 ABERDEEN PROVING GROUND MD 21005-5066
13	US ARMY RSRCH LAB ATTN IMNE ALC HRR MAIL & RECORDS MGMT ATTN RDRL CIM L TECHL LIB ATTN RDRL CIM P TECHL PUB ATTN RDRL SED P I LEE (10 COPIES) ADELPHI MD 20783-1197
TOTAL 22 (20 HCS, 1 CD, 1 ELEC)	

INTENITONALLY LEFT BLANK.